Applied Mathematical Modelling 37 (2013) 9732–9746

Contents lists available at SciVerse ScienceDirect

Applied Mathematical Modelling

journal homepage: www.elsevier.com/locate/apm

Mathematical modeling and computation of fire induced turbulent flow in partial enclosures

R. Harish, K. Venkatasubbaiah *

Department of Mechanical Engineering, Indian Institute of Technology Hyderabad, Hyderabad 502205, India

ARTICLE INFO

Article history:
Received 27 September 2012
Received in revised form 9 February 2013
Accepted 20 May 2013
Available online 5 June 2013

Keywords:
Fire-induced flow
Partial enclosure
Ceiling vent
Grashof number

ABSTRACT

The purpose of this paper is to understand the growth and spread of fires in ceiling vented enclosures. The transport phenomena due to fire have been modeled as buoyancy-induced turbulent flow in partial enclosures. The governing equations comprises the Reynolds averaged Navier–Stokes (RANS) equations with k—ϵ turbulence model in stream function–vorticity formulation approach. The governing equations are solved by high accuracy compact finite difference schemes with four stage Runge–Kutta method for time integration. Results are reported for Grashof numbers varied from 10^8 to 10^{10}. The effects of multiple heat sources in rectangular enclosure and ceiling vent aspect ratio in square enclosure are investigated. The thermal plume growth rate, ambient entrainment flow rate and the oscillatory nature at the vent opening are reported. As the Grashof number increases the effect of entrained ambient air is significant with higher volume flow rates through ceiling vent. A bidirectional flow is visualized at the ceiling opening. The distance between two heat sources governs the unified and independent behavior of thermal plumes. Present results are matching very well with the numerical and experimental results available in literature.

1. Introduction

Predictions of buoyancy induced thermal plume flow patterns inside vented enclosures has been interest of study because of their wide applications in thermal design of buildings, solar energy receivers and compartment fire propagation. The present study has wide implications on the risk assessment and fire safety management tasks for evaluating the adverse effects resulting from fire in buildings. In the context of fire safety in buildings, the first thing is to evacuate the smoke and heat released by the fire. Moreover the present study would help in fire safety measures such as location of smoke extraction fan system, location of fire and smoke detectors, location of smoke vent, smoke curtain or physical barriers, location of fire escape routes and evacuation modeling. The rate of inflow of oxygen from the ambient through openings has significant effect on the growth and spread of fire in buildings and to adjoining areas. The transport phenomena in buildings due to fire can be modeled as buoyancy-induced turbulent flow in partial enclosures.

One of the earliest studies by field models to predict fire behavior in compartments and aircraft cabins was presented by Markatos et al. [1–4]. The fire source is represented by volumetric heat source and transport phenomena due to fire is modeled as buoyancy induced turbulent flow in a two dimensional enclosure using K-epsilon turbulence model [1]. Later simulations were performed by Markatos and Pericleous [2] to predict the airflow and temperature distribution in a 3D compartment containing heat source. Their numerical predictions were compared with experimental observations and the capability of CFD to predict fire transport behavior was revealed. Keramida et al. [5] developed an integrated fire spread

* Corresponding author. Tel.: +91 4023016074; fax: +91 4023016032.
E-mail address: kvenkat@iith.ac.in (K. Venkatasubbaiah).

0307-904X/$ - see front matter © 2013 Elsevier Inc. All rights reserved.
http://dx.doi.org/10.1016/j.apm.2013.05.011

Nomenclature

H	height of the enclosure
D	width of the ceiling vent
W	width of the enclosure
T_s	heat source temperature
T_∞	initial fluid temperature
g	gravitational force per unit mass
t	time
u	velocity along x direction
v	velocity along y direction
β	coefficient of thermal expansion
α	thermal diffusivity
ν	kinematic viscosity
ν_t	turbulent eddy viscosity
Gr	Grashof number
Pr	Prandtl number
Pr_t	turbulent Prandtl number
k	turbulent Kinetic energy
ϵ	turbulent dissipation rate
ψ	stream function
ω	vorticity
Ψ	dimensionless stream function
Ω	dimensionless vorticity
θ	dimensionless temperature
U, V	dimensionless velocity components along X and Y directions
τ	dimensionless time
K	dimensionless turbulent kinetic energy
E	dimensionless turbulent dissipation rate

model by integrating the gaseous combustion model and thermal radiation model that has the capability of predicting the soot and pyrolysis effects.

Prahl and Emmons [6] studied the flow through doors and windows and incorporated mathematical models to predict the growth of enclosure fires. Abib and Jaluria [7] have numerically investigated the fire induced flow through a vertical opening in enclosure. The thermal plume behavior due to fire is modeled as buoyancy induced flow by Murgai and Emmons [8] and determined that the flow characteristics depends upon the size of fire and ambient conditions. Mercier and Jaluria [9] have experimentally depicted the fire-induced flow of smoke and hot gases in vertical open enclosure. Smoke and hot gases are injected into the enclosure from lower opening and the resulting downstream wall plume along the enclosure wall and flow fields are reported. In fire scenarios air flow rates through doorway was studied by Chow and Zou [10] using Large Eddy simulations. They have compared the empirical correlations on doorway flow rates with the experimental data. However, the above studies focus mainly on enclosures with vertical vents.

The horizontal vents are openings in ceilings, floors, stairwells, broken window at the top of atrium roof and smoke vent at the roof top. In horizontal vents the flow behavior is unstable and oscillatory when compared to vertical vents. Studies on the flow behavior of fire through horizontal vents are reported by Than and Savilonis [11] and Hinkley [12]. A comparison between the field model and experiment data in compartment with ceiling vent was performed by Kerrison et al. [13]. They have observed puff of hot gases from compartment fire with oscillatory behavior at the vent. Atkinson [14] studied experimentally the smoke movement driven by fire under a ceiling and observed rapidly rotating smoke rolls near the ceiling. Tan and Jaluria [15] performed experimental study on the mass flow rate through a horizontal vent in an enclosure and found a bidirectional flow arises across the vent due to buoyancy effects. Recently Venkatasubbaiah and Jaluria [16] numerically analyzed the enclosure fire with single and multiple horizontal vents. They have investigated within the laminar flow regime and found that the critical Grashof number is 10^6, above this flow becomes chaotic nature in the enclosure. The numerical investigations on enclosure fire with ceiling vents were limited.

The plume transport phenomena involves complex processes and it was studied by Lumley[17] and List[18]. They found that buoyancy induced turbulent mixing is important since it is one of the key process for the growth and spread of thermal plume. Laminar and turbulent natural convection was studied by Markatos and Pericleous [19] in a square cavity with differentially heated side walls using $k-\epsilon$ turbulence model. Abib and Jaluria [20] numerically analyzed the turbulent penetrative and recirculating flow in vented compartment fire with low Reynolds number model of Lam Bremhorst. Similarly Davidson [21] and Akhilesh et al. [22] carried out numerical analysis on buoyancy induced turbulent flows using Lam Bremhorst model and found that this model has higher capability of predicting turbulent quantities reasonably well in regions

near and away from the walls. Stavrakakis and Markatos [23] numerically studied the air flow in one and two room enclosures containing a fire source. The standard $k-\epsilon$ and RNG $k-\epsilon$ models were used to simulate the buoyancy induced flows. The capability of the two turbulence models were compared with the experimental results and it was concluded that both turbulence model can be used for fire simulations. The capability and accuracy of different turbulence models for the buoyancy induced turbulent flows were reported [24–26]. Several approaches have been proposed with better and optimized turbulence models [27–29]; however, there is no universal turbulence model that is suitable for all applications of computational fluid dynamics.

Patel and Markatos [30] carried out a detailed comparative study of eight discretization schemes by comparing the accuaracy, stability and CPU time requirements for a two-dimensional convection–diffusion equation. In recent years, there has been some interest in using high accuracy compact schemes for incompressible flows. Lele [31] have developed the compact finite difference schemes and it is found to be computationally efficient and yielded accurate results. Higher order compact finite difference scheme for unsteady two-dimensional convection–diffusion equation was proposed by Kalita and Chhabra [32] and it efficiently captured the transient and steady state solutions. Sengupta et al. [33] have developed high accuracy compact schemes for DNS and acoustics. Venkatasubbaiah and Sengupta [34] have applied compact schemes for DNS of mixed convection flow over a vertical plate. Recently Venkatasubbaiah and Jaluria [16] have implemented compact schemes for laminar natural convection flows in partial enclosure.

However, from literature the studies on the effects of multiple heat sources and ceiling vent aspect ratio in partial enclosures are limited. This has been the motivation for the present investigation. Here, the fire-induced turbulent flow in rectangular and square enclosures with ceiling vent is studied numerically using high accuracy compact schemes. The stream function and vorticity formulation with $k-\epsilon$ low Reynolds number turbulence model of Lam Bremhorst is used to solve the governing equations. Results are reported for different Grashof numbers. The effects of multiple heat sources in rectangular enclosure and ceiling vent aspect ratio of square enclosure are reported.

2. Governing equations and boundary conditions

The fire-induced turbulent flow in a rectangular and square enclosure with ceiling vent is shown in Fig. 1(a) and (b). There is a finite-size heat source at constant temperature T_s located at the bottom wall of enclosure with a ceiling vent of width D above the ambient media at temperature T_∞. The fire-induced flow is modeled as two-dimensional unsteady state incompressible buoyancy-induced turbulent flow in long rectangular and square enclosures with a ceiling vent. The governing equations for turbulent natural convection flows comprises the Reynolds averaged Navier–Stokes (RANS) equations, including the time averaged energy equation for the mean temperature field. The buoyancy term is modeled by Boussinesq approximation that treats density as a constant value in all equations, except for the buoyancy term in the momentum equation. In the present study the product of thermal expansion coefficient and temperature difference is less than 1 within the Boussinesq approximation limit. Turbulence is modeled with a low Reynolds number $k-\epsilon$ model of Lam Bremhorst including the contribution of buoyancy force in the turbulent kinetic energy generation and dissipation. The RANS equations for the velocity and temperature fields and $k-\epsilon$ turbulence model are as follows:

$$\frac{\partial u}{\partial x}+\frac{\partial v}{\partial y}=0, \tag{1}$$

$$\frac{\partial u}{\partial t}+u\frac{\partial u}{\partial x}+v\frac{\partial u}{\partial y}=-\frac{1}{\rho}\frac{\partial p}{\partial x}+\nu\left[\frac{\partial^2 u}{\partial x^2}+\frac{\partial^2 u}{\partial y^2}\right]+2\frac{\partial}{\partial x}\left[\nu_t\frac{\partial u}{\partial x}\right]+\frac{\partial}{\partial y}\left[\nu_t\frac{\partial u}{\partial y}\right]+\frac{\partial}{\partial y}\left[\nu_t\frac{\partial v}{\partial x}\right], \tag{2}$$

$$\frac{\partial v}{\partial t}+u\frac{\partial v}{\partial x}+v\frac{\partial v}{\partial y}=-\frac{1}{\rho}\frac{\partial p}{\partial y}+\nu\left[\frac{\partial^2 v}{\partial x^2}+\frac{\partial^2 v}{\partial y^2}\right]+\frac{\partial}{\partial x}\left[\nu_t\frac{\partial u}{\partial y}\right]+\frac{\partial}{\partial x}\left[\nu_t\frac{\partial v}{\partial x}\right]+2\frac{\partial}{\partial y}\left[\nu_t\frac{\partial v}{\partial y}\right]+g\beta(T-T_\infty), \tag{3}$$

$$\frac{\partial T}{\partial t}+u\frac{\partial T}{\partial x}+v\frac{\partial T}{\partial y}=\frac{\partial}{\partial x}\left[\left(\alpha+\frac{\nu_t}{\mathrm{Pr}_t}\right)\frac{\partial T}{\partial x}\right]+\frac{\partial}{\partial y}\left[\left(\alpha+\frac{\nu_t}{\mathrm{Pr}_t}\right)\frac{\partial T}{\partial y}\right], \tag{4}$$

$$\frac{\partial k}{\partial t}+u\frac{\partial k}{\partial x}+v\frac{\partial k}{\partial y}=\frac{\partial}{\partial x}\left[\left(\nu+\frac{\nu_t}{\sigma_k}\right)\frac{\partial k}{\partial x}\right]+\frac{\partial}{\partial y}\left[\left(\nu+\frac{\nu_t}{\sigma_k}\right)\frac{\partial k}{\partial y}\right]-\frac{g\beta\nu_t}{Pr_t}\frac{\partial T}{\partial y}-\epsilon+\nu_t\left[2\left(\frac{\partial u}{\partial x}\right)^2+2\left(\frac{\partial v}{\partial y}\right)^2+\left(\frac{\partial u}{\partial y}+\frac{\partial v}{\partial x}\right)^2\right], \tag{5}$$

$$\begin{aligned}\frac{\partial \epsilon}{\partial t}+u\frac{\partial \epsilon}{\partial x}+v\frac{\partial \epsilon}{\partial y}=&\frac{\partial}{\partial x}\left[\left(\nu+\frac{\nu_t}{\sigma_\epsilon}\right)\frac{\partial \epsilon}{\partial x}\right]+\frac{\partial}{\partial y}\left[\left(\nu+\frac{\nu_t}{\sigma_\epsilon}\right)\frac{\partial \epsilon}{\partial y}\right]-C_{2\epsilon}f_2\frac{\epsilon^2}{k}\\&+C_{1\epsilon}f_1\left[\nu_t\left\{2\left(\frac{\partial u}{\partial x}\right)^2+2\left(\frac{\partial v}{\partial y}\right)^2+\left(\frac{\partial u}{\partial y}+\frac{\partial v}{\partial x}\right)^2\right\}-C_{3\epsilon}\left\{\frac{g\beta\nu_t}{Pr_t}\frac{\partial T}{\partial y}\right\}\right],\end{aligned} \tag{6}$$

where g is the acceleration due to gravity; β is the coefficient of volumetric thermal expansion; ρ is the density of the fluid; ν is the kinematic viscosity; α is the thermal diffusivity; ν_t is the turbulent eddy viscosity; Pr_t is the turbulent Prandtl number.

For low Reynolds number $k-\epsilon$ turbulence model, constants used are $C_\mu=0.09$, $C_{1\epsilon}=1.44$, $C_{2\epsilon}=1.92$, $C_{3\epsilon}=0.7$, $Pr_t=0.9$, $\sigma_k=1.0$, $\sigma_s=1.3$. The damping wall functions f_1, f_2 and f_μ are as follows.

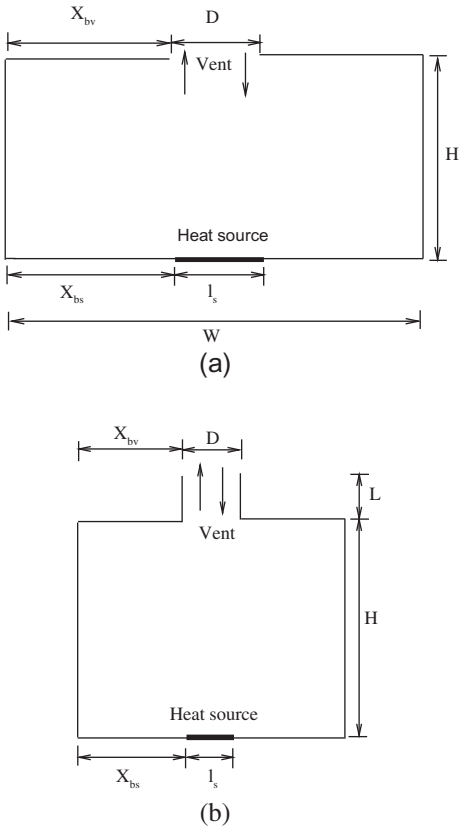

Fig. 1. Schematic diagram of partial enclosures: (a) rectangular and (b) square.

$$f_1 = 1 + \left(\frac{0.14}{f_\mu}\right)^3, \tag{7}$$

$$f_2 = \left[1 - 0.27\exp(-R_t^2)\right][1 - \exp(-R_n)], \tag{8}$$

$$f_\mu = \exp\left[-\frac{3.4}{1 + \left(\frac{R_t}{50}\right)^2}\right], \tag{9}$$

where $R_t = \frac{k^2}{\nu\epsilon}$, $R_n = \frac{k^{\frac{1}{2}}n}{\nu}$; n is the normal distance from the nearest wall.

The RANS equations are obtained in the stream function (ψ) and vorticity (ω) formulation. Advantages of this formulation are added accuracy due to exact satisfaction of mass conservation and reduction in the number of unknowns to two as compared to three unknowns for primitive variable formulation. Pressure is eliminated by taking the curl of the momentum equation to give the vorticity transport equation (VTE).

The dimensionless governing equations are obtained by the following variables: $X = \frac{x}{H}$, $Y = \frac{y}{H}$, $U = \frac{u}{V_c}$, $V = \frac{v}{V_c}$, $\tau = \frac{tV_c}{H}$, $\theta = \frac{T-T_\infty}{T_s-T_\infty}$, $V_c = (g\beta\Delta TH)^{\frac{1}{2}}$, $\Omega = \omega\frac{(H)^{\frac{1}{2}}}{(g\beta\Delta T)^{\frac{1}{2}}}$, $\Psi = \frac{\psi}{(g\beta\Delta TH^3)^{\frac{1}{2}}}$, $K = \frac{k}{(g\beta\Delta TH)}$, $E = \frac{\epsilon}{((g\beta\Delta T)^3H)^{\frac{1}{2}}}$.

The dimensionless buoyancy-induced turbulent flow equations are as follows:

$$\frac{\partial^2\Psi}{\partial X^2} + \frac{\partial^2\Psi}{\partial Y^2} = -\Omega, \tag{10}$$

$$\frac{\partial\Omega}{\partial\tau} + U\frac{\partial\Omega}{\partial X} + V\frac{\partial\Omega}{\partial Y} = \frac{\partial^2}{\partial X^2}\left[\left(\frac{1}{(Gr)^{\frac{1}{2}}} + \frac{1}{Re_t}\right)\Omega\right] + \frac{\partial\theta}{\partial X} + \frac{\partial^2}{\partial Y^2}\left[\left(\frac{1}{(Gr)^{\frac{1}{2}}} + \frac{1}{Re_t}\right)\Omega\right] + 2\frac{\partial U}{\partial Y}\frac{\partial^2}{\partial X^2}\left[\frac{1}{Re_t}\right] - 2\frac{\partial V}{\partial X}\frac{\partial^2}{\partial Y^2}\left[\frac{1}{Re_t}\right] + 2\left[\frac{\partial V}{\partial Y} - \frac{\partial U}{\partial X}\right]\frac{\partial^2}{\partial X\partial Y}\left[\frac{1}{Re_t}\right], \tag{11}$$

$$\frac{\partial\theta}{\partial\tau} + U\frac{\partial\theta}{\partial X} + V\frac{\partial\theta}{\partial Y} = \frac{\partial}{\partial X}\left[\left(\frac{1}{(Pr(Gr)^{\frac{1}{2}}} + \frac{1}{Pr_tRe_t}\right)\frac{\partial\theta}{\partial X}\right] + \frac{\partial}{\partial Y}\left[\left(\frac{1}{(Pr(Gr)^{\frac{1}{2}}} + \frac{1}{Pr_tRe_t}\right)\frac{\partial\theta}{\partial Y}\right], \tag{12}$$

$$\frac{\partial K}{\partial \tau}+U\frac{\partial K}{\partial X}+V\frac{\partial K}{\partial Y}=\frac{\partial}{\partial X}\left[\left(\frac{1}{(Gr)^{\frac{1}{2}}}+\frac{1}{\sigma_k Re_t}\right)\frac{\partial K}{\partial X}\right]+\frac{\partial}{\partial Y}\left[\left(\frac{1}{(Gr)^{\frac{1}{2}}}+\frac{1}{\sigma_k Re_t}\right)\frac{\partial K}{\partial Y}\right]-\frac{1}{Re_t Pr_t}\frac{\partial \theta}{\partial Y}-E+\frac{1}{Re_t}\left[2\left(\frac{\partial U}{\partial X}\right)^2+2\left(\frac{\partial V}{\partial Y}\right)^2+\left(\frac{\partial U}{\partial Y}+\frac{\partial V}{\partial X}\right)^2\right], \tag{13}$$

$$\frac{\partial E}{\partial \tau}+U\frac{\partial E}{\partial X}+V\frac{\partial E}{\partial Y}=\frac{\partial}{\partial X}\left[\left(\frac{1}{(Gr)^{\frac{1}{2}}}+\frac{1}{\sigma_\epsilon Re_t}\right)\frac{\partial E}{\partial X}\right]+\frac{\partial}{\partial Y}\left[\left(\frac{1}{(Gr)^{\frac{1}{2}}}+\frac{1}{\sigma_\epsilon Re_t}\right)\frac{\partial E}{\partial Y}\right]-C_{2_\epsilon}f_2\frac{E^2}{K}+C_{1_\epsilon}f_1\left[\frac{1}{Re_t}\left\{2\left(\frac{\partial U}{\partial X}\right)^2+2\left(\frac{\partial V}{\partial Y}\right)^2+\left(\frac{\partial U}{\partial Y}+\frac{\partial V}{\partial X}\right)^2\right\}+C_{3_\epsilon}\left\{-\frac{1}{Re_t Pr_t}\frac{\partial \theta}{\partial Y}\right\}\right]\frac{E}{K}, \tag{14}$$

where $Gr=\frac{g\beta\Delta TH^3}{\nu^2}$ is the Grashof number; $Re_t=\frac{E}{C_\mu f_\mu K^2}$.

The expressions for the velocity components in terms of stream function are as follows.

$$U=\frac{\partial \psi}{\partial Y},\quad V=-\frac{\partial \psi}{\partial X}. \tag{15}$$

It is easy to describe the boundary conditions at the solid walls. The problem is, however, the treatment of the boundaries that are not bounded by solid walls and that involve entrainment flows at the openings. Mass, momentum and energy exchange may take place at the opening as a result of viscous effects and turbulent mixing. The boundary conditions at the opening have to consider the interactions between cold and hot fluids due to temperature difference. Hence flow modeling in enclosure with ceiling vent is complex due to bidirectional flow at the vent. Chan and Tian [35] reported fairly accurate results by restricting the calculations within the cavity. In the present study the computational domain is restricted within the cavity. No-slip boundary condition is applied on the solid walls for the velocity field. The temperature of the source is specified and the remaining walls are taken as adiabatic for temperature field. At the vent horizontal velocity is set to zero and normal gradients are specified for temperature, vertical velocity, kinetic energy and dissipation.

The appropriate initial and boundary conditions in dimensionless form are as follows:

$$\text{at } \tau=0: \quad \psi=\text{constant};\ \Omega=\theta=0. \tag{16}$$

For $\tau>0$:

$$X=0;\ X=2.0;\ 0<Y<1.0: \quad \psi=\text{constant};\ \Omega=-\frac{\partial^2\psi}{\partial X^2};\ \frac{\partial \theta}{\partial X}=0;\ K=0;\ \frac{\partial E}{\partial X}=0, \tag{17}$$

$$Y=0;\ 0<X<2.0: \quad \psi=\text{constant};\ \Omega=-\frac{\partial^2\psi}{\partial Y^2};\ K=0;\ \frac{\partial E}{\partial Y}=0,$$

$$Y=0;\ 0<X<X_{bs}: \quad \frac{\partial \theta}{\partial Y}=0,$$

$$X_{bs}<X<X_{bs}+l_s: \quad \theta=1.0,$$

$$X_{bs}+l_s<X<2.0: \quad \frac{\partial \theta}{\partial Y}=0, \tag{18}$$

$$Y=1.0;\ 0<X<X_{bv}: \quad \psi=\text{constant};\ \Omega=-\frac{\partial^2\psi}{\partial Y^2};\ \frac{\partial \theta}{\partial Y}=0,$$

$$K=0;\ \frac{\partial E}{\partial Y}=0,$$

$$X_{bv}<X<X_{bv}+D: \quad \frac{\partial \psi}{\partial Y}=\frac{\partial \Omega}{\partial Y}=\frac{\partial \theta}{\partial Y}=\frac{\partial K}{\partial Y}=\frac{\partial E}{\partial Y}=0,$$

$$X_{bv}+D<X<2.0: \quad \psi=\text{constant};\ \Omega=-\frac{\partial^2\psi}{\partial Y^2};\ \frac{\partial \theta}{\partial Y}=0,$$

$$K=0;\ \frac{\partial E}{\partial Y}=0, \tag{19}$$

where X_{bs} is the distance up to the source; l_s is the source width; X_{bv} is the distance up to the vent; D is the vent width; W is the width of the enclosure.

3. Method of solution

The governing equations are discretized using finite difference schemes and the solver is developed in Fortran 90. The stream function equation (SFE) is discretized using a second order central difference scheme (CD_2). An iteration method

of Bi-conjugate gradient is used to solve the stream function equation. The vorticity transport equation (VTE), energy equation (EE), Kinetic energy and dissipation equations are solved by discretizing the diffusion terms using CD_2. Time integration is performed explicitly by the four stage Runge–Kutta (RK4) scheme and nonlinear convection terms are discretized by high accuracy compact schemes, whose details are given in Sengupta et al. [33]. All simulations are performed with double precision to reduce the round-off error. The convergence criterion is chosen as $\leqslant 10^{-8}$ to solve the stream function equation. A small time step of $\Delta\tau = 10^{-4}$ is chosen to avoid the numerical instability. The CPU time required for a typical run was around 30 h with an Intel Xenon workstation of 2.27 GHz and 12 GB RAM.

4. Validation and grid independence

The accuracy of the present numerical model and method of solution has been tested with the experimental and numerical results available in the literature. Dixit and Babu [36] have numerically analyzed the buoyancy driven flow in a square cavity that has a differentially heated vertical walls and adiabatic upper and bottom walls by lattice Boltzmann method (LBM) for Rayleigh number $Ra = 10^7$. The stream function and temperature contours shown in Fig. 2(a) and (b) are matching well with the numerical results of Dixit and Babu [36]. Fig. 2(c) depicts the temperature profile along the horizontal wall at the center of the enclosure and shows quantitative comparison between the present results and LBM results reported by Dixit and Babu [36]. The average Nusselt number is evaluated by integrating the local Nusselt number along the left hot wall. The average Nusselt number comparison presented in Table 1 shows good agreement with the results of Dixit and Babu [36] and Markatos and Pericleous [19]. The experimental study on the natural convection flow in a square cavity that has a differentially heated vertical walls and adiabatic upper and bottom walls for $Ra = 1.58 \times 10^9$ was reported by Tian and Karayiannis [37]. Fig. 2(d) and (e) shows the temperature and velocity profiles along the horizontal wall at the center of the square enclosure for $Ra = 1.58 \times 10^9$ and gives a quantitative comparison between compact scheme, CD_2 and with the experimental results. It is noticed that the present results with compact schemes are accurate than CD_2 and are closer to the experimental results of Tian and Karayiannis [37].

Fig. 3(a)–(c) shows the temperature, horizontal and vertical velocity profiles along vertical axis at $x = 0.25H$ from left wall for different grid sizes of 200×100, 300×150 and 400×200 for $Gr = 10^{10}$. From Fig. 3, it is noticed that the solution is grid independent with grid size of 300×150. Similarly the velocity and temperature profiles are grid independent at different locations. Moreover the wall y^+ value calculated is less than 1 and hence all simulations are reported with this grid size.

5. Results and discussion

The fire-induced turbulent flow in rectangular and square enclosures with ceiling or horizontal vent is numerically studied and presented for different Grashof numbers. The effects of multiple heat sources in rectangular enclosure and ceiling vent aspect ratio of square enclosure on the flow flied characteristics are presented. Here, the value of Prandtl number Pr of air is taken as 0.72 for all the cases. The width of the rectangular enclosure is $W = 2H$, with ceiling vent width $D = 0.2H$ and heat source size $l_s = 0.2H$. Present analysis is valid as long as the product of thermal expansion coefficient and temperature difference is less than one. The height of the enclosure is chosen as 0.8 m and the product of thermal expansion coefficient and temperature difference are within the Boussinesq approximation limit for $Gr = 10^8$ to 10^{10}.

To know the flow evolution with time in a vented rectangular enclosure, stream function, temperature, kinetic energy and normal velocity contours at different times are shown in Fig. 4 for $Gr = 10^8$. The heat source is located at the center of the bottom wall with size $l_s = 0.2H$ and vent of size $D = 0.2H$ at the center of the ceiling. From Fig. 4, the stream function contours and thermal plume move upwards from the heat source with increase in time. The flow reaches the ceiling vent at time $\tau = 15$. A density difference arises between the inner (hot) fluid and the outer (cold) fluid at the vent. The flow is bidirectional at the vent due to the buoyancy effect. From Fig. 4(c), a region of recirculation is formed in the cavity due to the interactions between the warmer fluid rising from the heat source to the cold fluid entering the enclosure through the vent. The intensity of thermal plume increases with increase in time and it reaches the ceiling and spreads downwards as shown in Fig. 4(d)–(f). The hot air travels against the ventilated air current whereas the fresh air enters and travels towards the fire source, leading to an excessive flow rotation and eventually an effective mixing of plume and fresh air is visualized inside the enclosure at time $\tau = 100$. This creates more turbulence and leading to well mixed environment inside the enclosure as depicted through the kinetic energy contour plot shown in Fig. 4(g). From Fig. 4(h) the normal velocity contours depicts the rising thermal plume with positive values and entrained ambient air with negative values. The normal velocity contours shows the symmetrical entrainment of air from both sides of the rising central plume and the entrained ambient air gets heated up quickly which assists the plume to spread at a higher rate inside the enclosure.

The stream function, temperature, kinetic energy and normal velocity contours in a vented rectangular enclosure at time $\tau = 100$ are shown in Fig. 5 for $Gr = 10^{10}$. The heat source of size $l_s = 0.2H$ size and vent of width $D = 0.2H$ are placed at the center of bottom wall and ceiling. From Fig. 5 as Gr increases from 10^8 to 10^{10}, the flow characteristics are highly transient, unstable and complex inside the enclosure due to increase of buoyancy. As Grashof number increases, the cold air creeps in at a faster rate into the enclosure through the vent. Hence increase in circulations and well mixing of hot air and cold air are visualized inside the enclosure. When Gr is increased to 10^{10}, the heat source temperature increases thereby increasing the intensity and strength of the thermal plume, hence the plume oscillates and leaves the enclosure at a higher rate. From

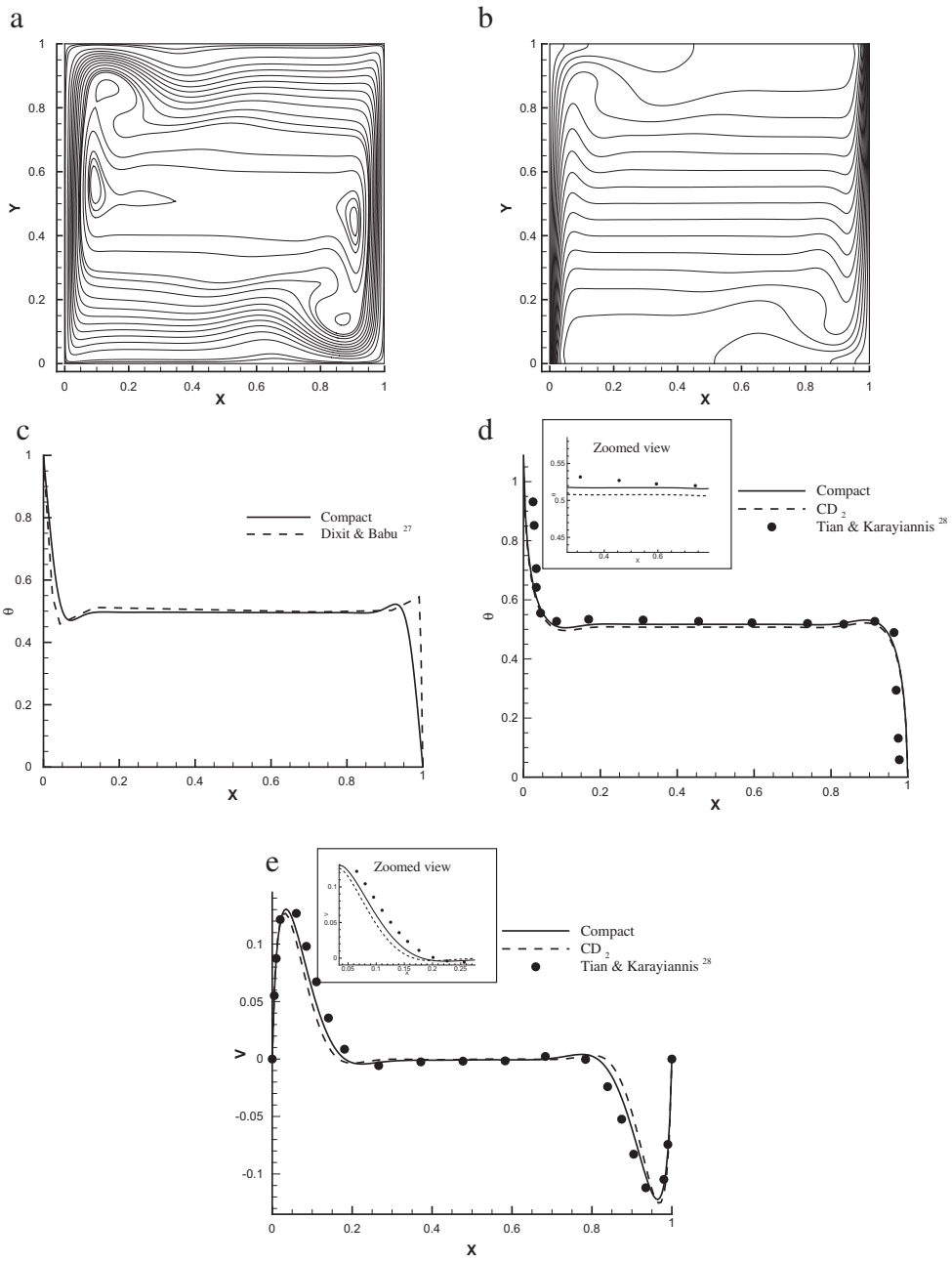

Fig. 2. Validation of present results with: LBM (a–c); Experimental (d, e).

Fig. 5(c) and (d), the intensity of turbulent kinetic energy and normal velocity increases. In Fig. 5(e), the normal velocity profile is plotted along the vent at different times for $Gr = 10^{10}$. The normal velocity increases with increase in time, hence the volume flow rate through the vent increases. Flow is oscillating and bidirectional at the vent due to buoyancy. From Fig. 5(f), with higher value of $Gr = 10^{10}$ the magnitude and oscillations of instantaneous normal velocity at the vent center point increases hence the intensity of turbulence increases.

The flow characteristics in a vented rectangular enclosure with two heat sources of equal size $l_s = 0.2H$ placed at $0.4H$ and $1.4H$ from the left wall are shown in Fig. 6 for $Gr = 10^8$. The vent is centrally located with width $D = 0.2H$. Fig. 6(a)–(c) represents the stream function contours, (d–f) temperature contours and (g, h) turbulent kinetic energy contours. From Fig. 6, at $\tau = 10$ one can notice two axisymmetric plumes rising from the heat sources towards the ceiling. As time progresses quiescent and cool ambient air is entrained through the vent and mixes with the rising plumes as they continue their ascent towards the ceiling. Meanwhile the two plumes escapes through the vent and conjunction is formed between two plumes. At

Table 1
Average Nusselt number on the heated wall.

Rayleigh number	Present	Dixit and Babu [36]	Markatos and Pericleous [19]
10^7	16.837	16.79	–
10^8	30.952	30.506	32.045

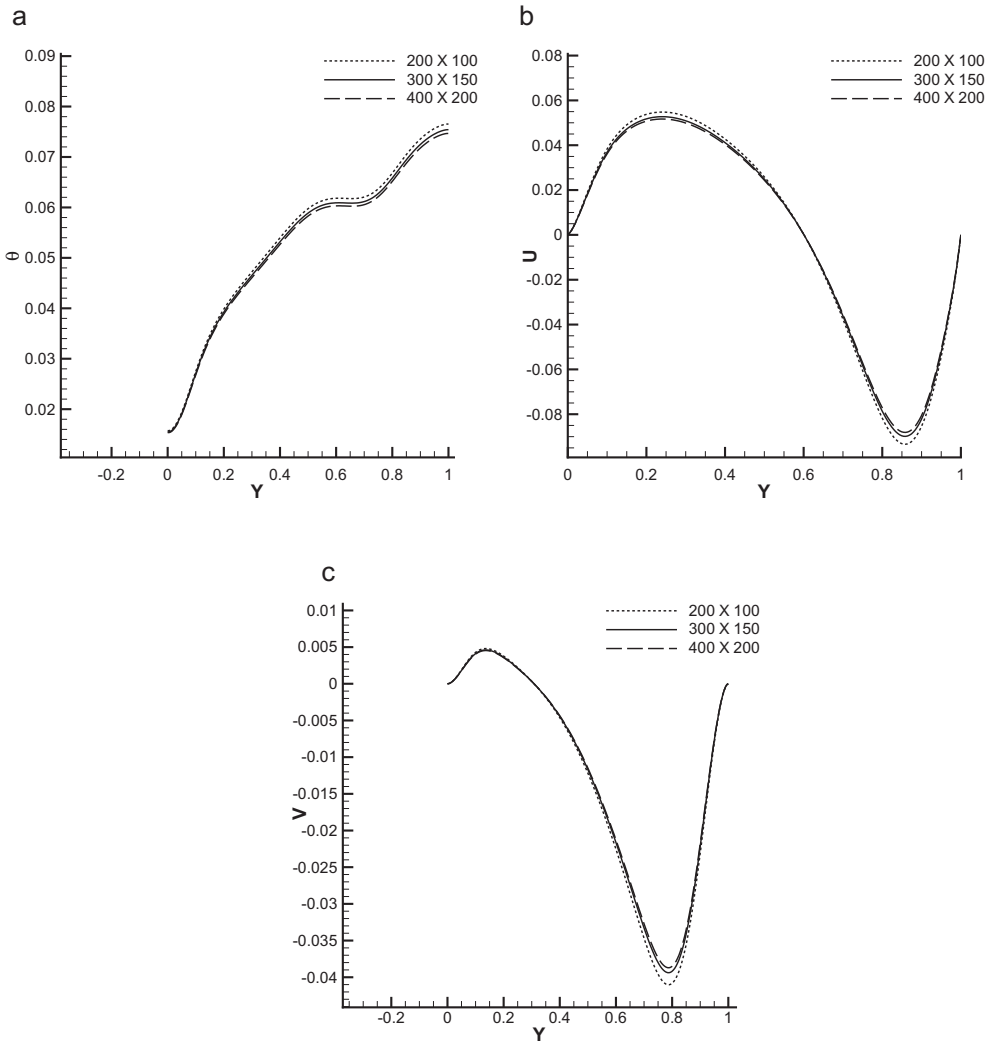

Fig. 3. (a) Temperature profile, (b) horizontal velocity and (c) vertical velocity profiles along the vertical axis for different grid sizes.

$\tau = 15$ the turbulent kinetic energy contour shows that the fluid circulates within the cavity by a vortex formation and leaves through the vent. The entrained air interacts with rising plumes and creates a well-mixed environment as visualized in the stream function, kinetic energy and temperature contours at $\tau = 50$. As the flow evolves the movement of the second plume is more vigorous towards the first plume and the interactions are higher between the two plumes.

To know the effect of heat source locations in a vented rectangular enclosure, the temperature contours are shown in Fig. 7 for $Gr = 10^8$. The two heat sources are of size $0.2H$ placed at $0.7H$ and $1.1H$ from the left wall with a centrally located ceiling vent of width $D = 0.2H$. At initial time $\tau = 2$ two axisymmetric plumes rises from the heat sources and are unified at $\tau = 5$. As time progresses the plumes are unified and evolves as a single plume rising towards the ceiling. A similar phenomenon was observed experimentally by Ichimiya and Saiki [38]. Fig. 7(e, f) shows the comparison of temperature and normal velocity profiles along the horizontal wall at the center of the rectangular enclosure for three different cases of a centrally located single heat source and two heat source separated by a distance of $0.8H$ and $0.2H$. From Fig. 7 (e, f), the temperature and normal velocity increases with decrease in distance between two heat sources due to early unification of plumes. When

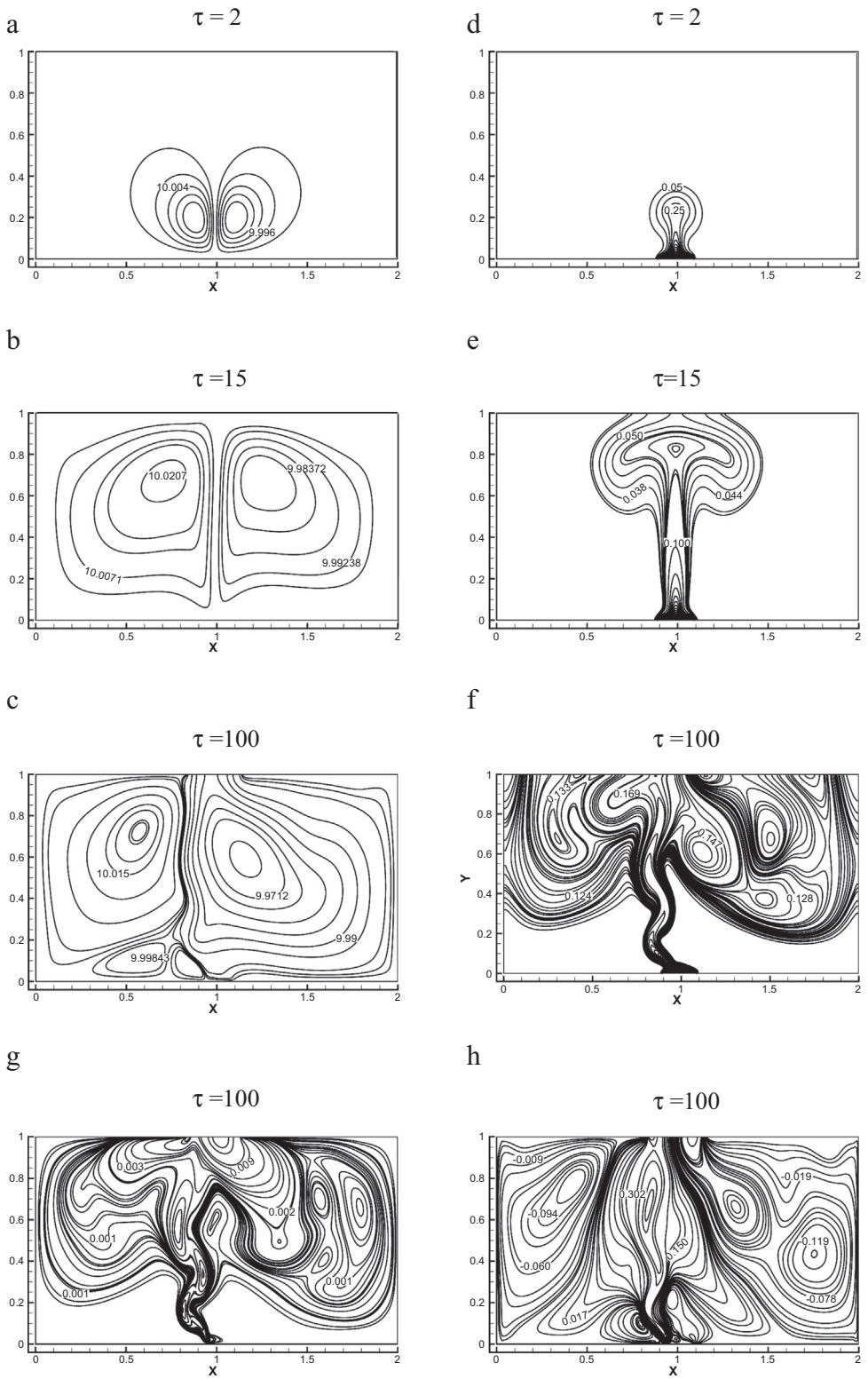

Fig. 4. Evolution of stream function (a–c), temperature (d–f), kinetic energy (g) and vertical velocity (h) contours for $Gr = 10^8$.

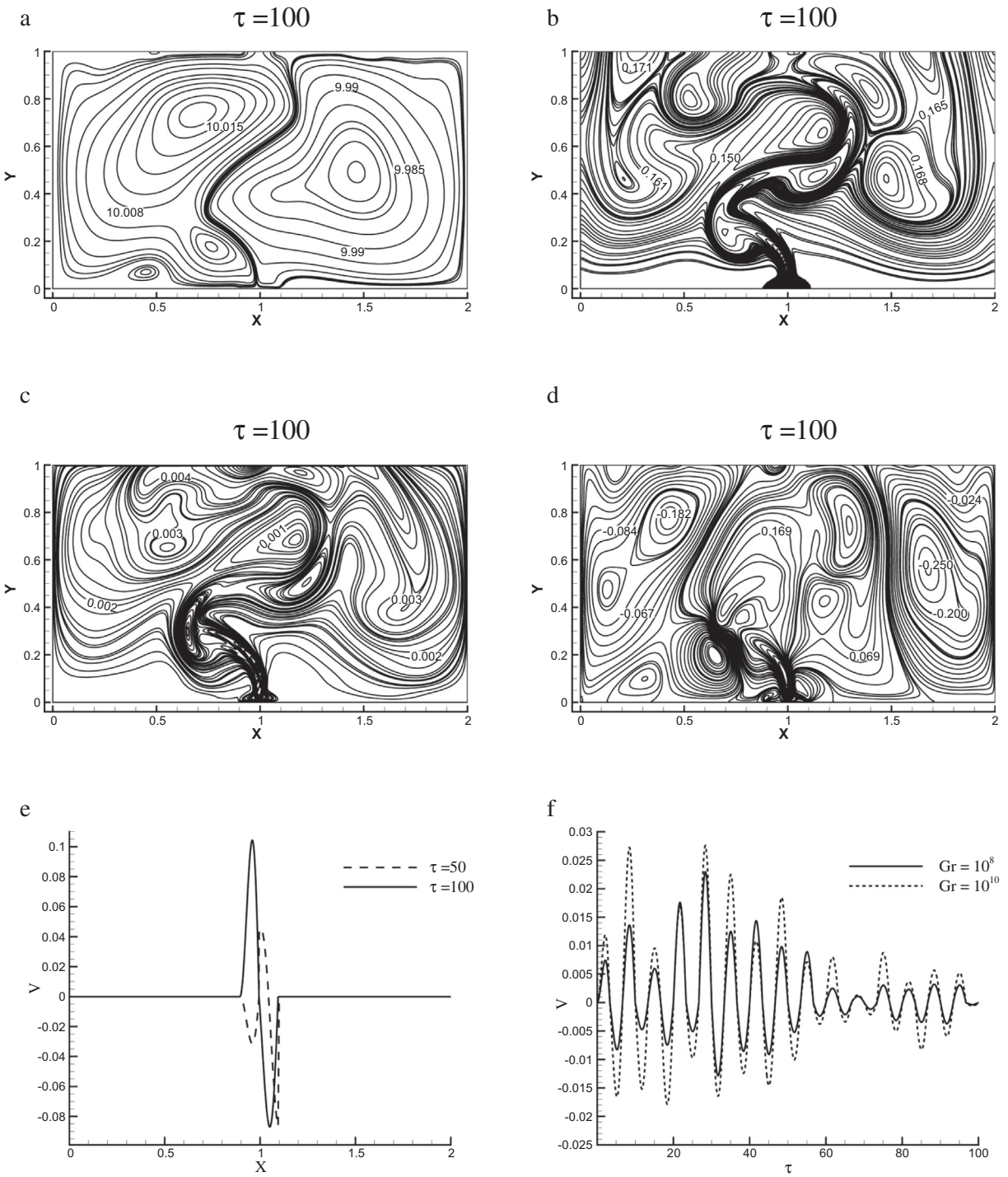

Fig. 5. Stream function (a), temperature (b), kinetic energy (c) and vertical velocity (d) contours, (e) Normal velocity profile along the vent for $Gr = 10^{10}$. (f) Instantaneous normal velocity variation at the center of the vent.

the distance between the two heat sources are increased from 0.2*H* to 0.8*H* the two thermal plumes are independent and moves separately towards the ceiling. The normal velocity for single heat source is higher when compared to two heat sources separated by a distance of 0.8*H* since the ceiling vent is located above the single heat source. Moreover the entrained air has to take a longer path to interact with the two rising plumes. From Fig. 6 and 7, it can be concluded that the distance between two heat sources and ceiling vent location governs the growth and spreading of fires inside the buildings.

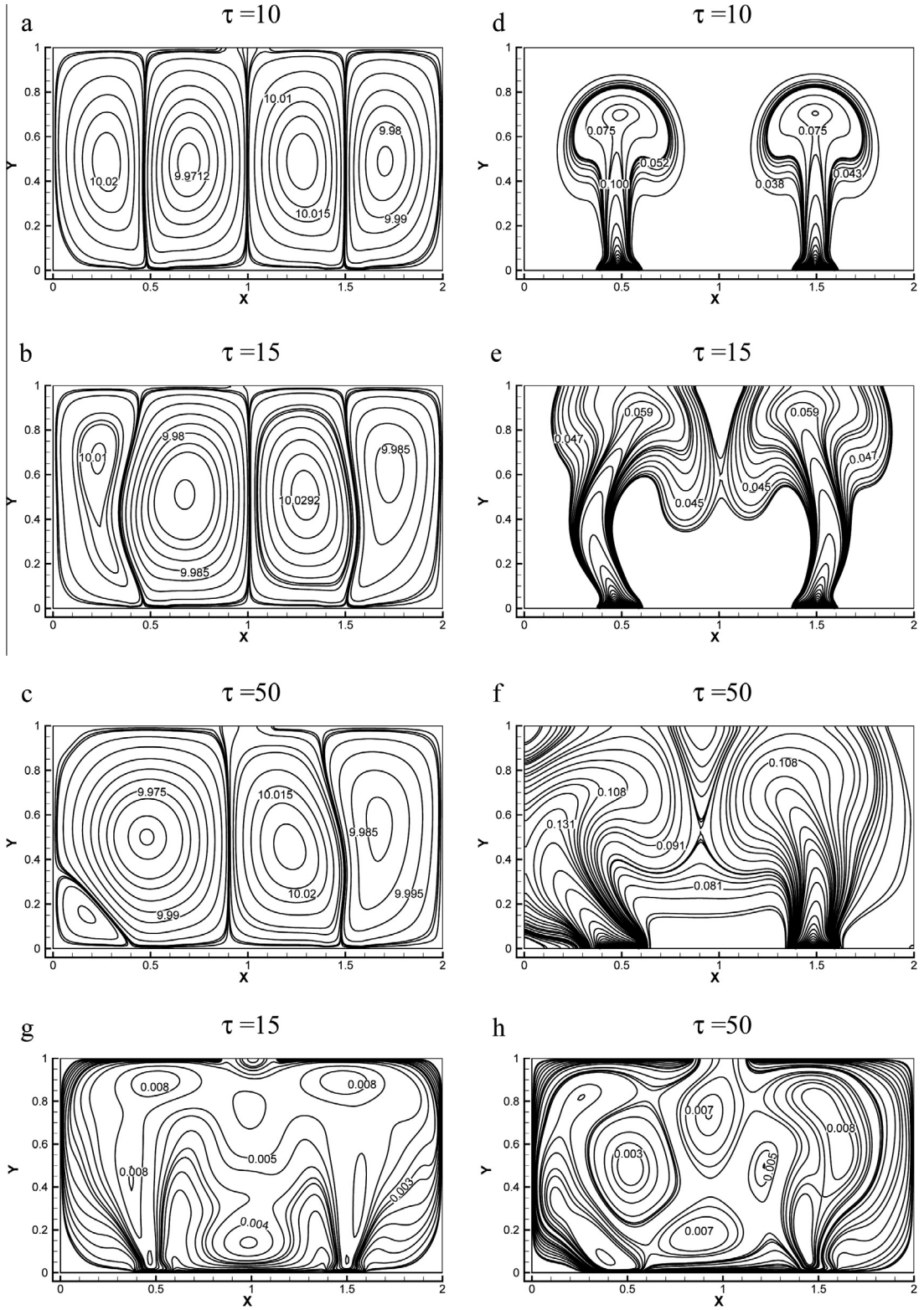

Fig. 6. Stream function (a–c), temperature (d–f), kinetic energy (g, h) for two heat sources of equal size $l_s = 0.2H$ located at $0.4H$ and $1.4H$ at $Gr = 10^8$.

Fig. 8 shows the effect of ceiling vent aspect ratio in a square enclosure with stream function, temperature and turbulent kinetic energy contours for $Gr = 10^8$. The centrally located heat source and vent are of size $l_s = 0.2H$, $D = 0.2H$ with vent thickness $L = 0.2H$. From Fig. 8(a) and (b) as time progresses the stream function contours move upwards and a region of recirculation is formed in the vent due to interactions between hot and cold fluids. In Fig. 8(c) and (d) the entrained air tilts the thermal plume towards the left wall. As the flow evolves with time, the turbulent kinetic energy is attributed to the fluctuation of the upward rising turbulent thermal plume. From Fig. 8(e) at $\tau = 25$ the kinetic energy contours depicts the interaction between the hot air and counter cold air at the vent generating swirl flow motion near the ceiling opening and as flow evolves more circulations are visualized near the left wall due to tilting of the thermal plume. The normal velocity and temperature profile along the vent top for different vent thicknesses are shown in Fig. 8(g) and (h). The normal velocity and temperature increases with decrease in vent thickness since the hot and cold fluid interactions occur quickly hence increases the

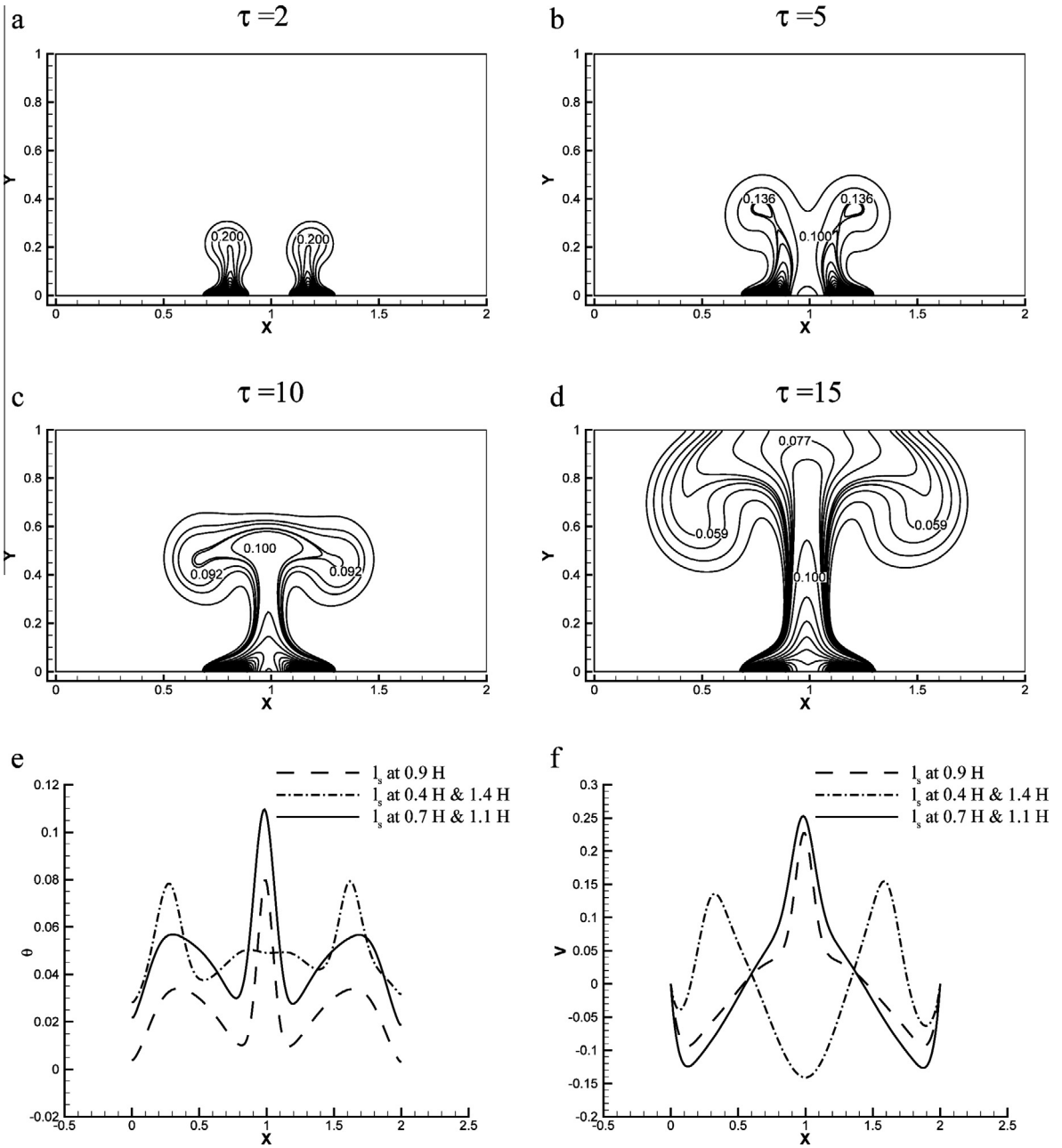

Fig. 7. Temperature contours (a–d) for two heat sources of equal size $l_s = 0.2H$ located at $0.7H$ and $1.1H$ at $Gr = 10^8$; Comparison of mid-height temperature (e) and normal velocity (f) profiles variations along X-direction.

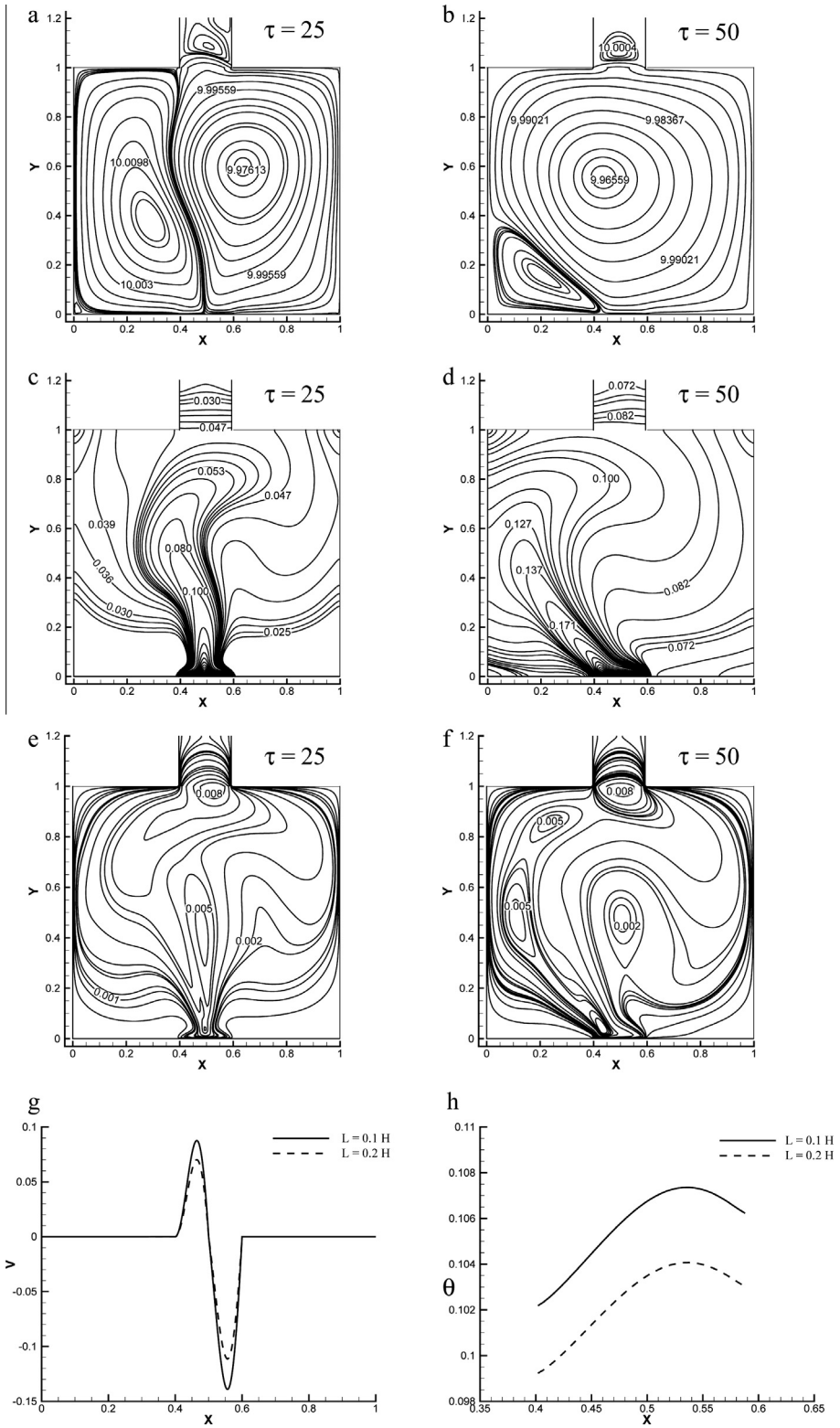

Fig. 8. Stream function (a, b), temperature (c, d), kinetic energy (e, f) contours in a square enclosure for $Gr = 10^8$. Variation of normal velocity (g) and temperature (h) profiles along the top vent with different vent thickness.

volume flow rate through the vent. Similarly Mercer and Thompson [39] have observed experimentally that the volume flow rate decreases with increase in vent thickness.

6. Conclusions

The buoyancy-induced turbulent flow generated by a heat source such as fire in rectangular and square enclosures with ceiling vent has been investigated numerically. The fluid flow characteristics in the enclosures are reported for various parameters such as Grashof number, multiple heat sources and vent aspect ratio. The flow is found to be oscillating and bidirectional at the vent due to buoyancy effects. As the Grashof number increases from 10^8 to 10^{10}, the flow becomes highly transient, unstable and chaotic in the enclosure due to increase of buoyancy. The intensity of turbulence increases with increase in Grashof number, increasing the entrained ambient air flow rate through the vent. The two thermal plumes get unified and propagates as a single thermal plume when two heat sources are separated by a distance $\leqslant 0.2H$. The intensity of thermal plume is higher when two plumes are unified. The distance between the two heat sources and ceiling vent location governs the growth and spreading of fires in the vented enclosures. The volume flow rate through the vent increases with decrease in vent thickness. Present results would be useful for understanding the growth and spread of fire and guidance for devising effective fire safety systems in buildings.

References

[1] N.C. Markatos, M.R. Malin, Mathematical modeling of buoyancy-induced smoke flow in enclosures, Int. J. Heat Mass Transfer 25 (1982) 63–75.
[2] N.C. Markatos, K.A. Pericleous, An investigation of three-dimensional fires in enclosures, Rev. Gen. Thermiquel. 23 (1984) 66–78.
[3] E.R. Galea, N.C. Markatos, A review of mathematical modelling of aircraft cabin fires, Appl. Math. Model. 11 (1987) 162–176.
[4] E.R. Galea, N.C. Markatos, The mathematical modelling and computer simulation of fire development in aircraft, Int. J. Heat Mass Transfer 34 (1991) 181–197.
[5] E.P. Keramida, N.N. Souris, A.G. Boudouvis, N.C. Markatos, Numerical Modeling of Radiative Heat Transfer in Integrated CFD Fire Modeling, J. Appl. Fire Sci. 9 (2000) 3–19.
[6] J. Prahl, H.W. Emmons, Fire induced flow through an opening, Combust. Flame 25 (1975) 369–385.
[7] A.H. Abib, Y. Jaluria, Numerical simulation of the buoyancy induced flow in a partially open enclosure, Numer. Heat Transfer 14 (1988) 235–254.
[8] M.P. Murgai, H.W. Emmons, Natural convection above fires, J. Fluid Mech. 8 (1960) 611–624.
[9] G.P. Mercier, Y. Jaluria, Fire-induced flow of smoke and hot gases in open vertical Enclosures, Exp. Therm. Fluid. Sci. 19 (1999) 77–84.
[10] W.K. Chow, G.W. Zou, Correlation equations on fire-induced air flow rates through doorway derived by large eddy simulation, Build. Environ. 40 (2005) 897–906.
[11] C.F. Than, B. Savilonis, Modelling fire behaviour in an enclosure with a ceiling vent, Fire Safety J. 20 (1993) 151–174.
[12] P.L. Hinkley, Rates of production of hot gases in roof venting experiments, Fire Safety J. 10 (1986) 57–65.
[13] L. Kerrison, E.R. Galea, M.K. Patel, A Two-dimensional Numerical Investigation of the Oscillatory Flow Behaviour in Rectangular Fire Compartments with a Single Horizontal Ceiling Vent, Fire Safety J. 30 (1988) 357–382.
[14] Graham Atkinson, Smoke movement driven by a fire under a ceiling, Fire Safety J. 25 (1995) 261–275.
[15] Qing Tan, Yogesh Jaluria, Mass Flow through a horizontal vent in an enclosure due to pressure and density differences, Int. J. Heat Mass Transfer 44 (2001) 1543–1553.
[16] K. Venkatasubbaiah, Y. Jaluria, Numerical simulation of enclosure fires with horizontal vents, Numer. Heat Transfer A 62 (2012) 179–196.
[17] J.L. Lumley, Explanation of thermal plume growth rate, Phys. Fluids 14 (1971) 2537.
[18] E.J. List, Turbulent jets and plumes, Annu. Rev. Fluid Mech. 14 (1982) 189–212.
[19] N.C. Markatos, K.A. Pericleous, Laminar and turbulent natural convection in an enclosed cavity, Int. J. Heat Mass Transfer 27 (1984) 755–772.
[20] A.H. Abib, Y. Jaluria, Turbulent penetrative and recirculating flow in a compartment fire, J. Heat Transfer 117 (1995) 927–935.
[21] Lars Davidson, Calculation of the turbulent buoyancy driven flow in a rectangular cavity using an efficient solver and two different low reynolds number k—ϵ turbulence models, Numer. Heat Transfer A 18 (1990) 129–147.
[22] Akhilesh Gupta, V. Eswaran, Prabhat Munshi, N.K. Maheshwari, P.K. Vijayan, Thermal stratification studies in a side heated water pool for advanced heavy water reactor applications, Heat Mass Transfer 45 (2009) 275–285.
[23] G.M. Stavrakakis, N.C. Markatos, Simulation of airflow in one- and two-room enclosures containing a fire source, Int. J. Heat Mass Transfer 52 (2009) 2690–2703.
[24] S. Gavrilakis, Numerical simulation of low-Reynolds-number turbulent flow through a straight square duct, J. Fluid Mech. 244 (1992) 101–129.
[25] Karim Van Maele, Bart Merci, Application of two buoyancy-modified k—ϵ turbulence models to different types of buoyant plumes, Fire Safety J. 41 (2006) 122–138.
[26] S.J. Wang, A.S. Mujumdar, A comparative study of five low Reynolds number k—ϵ models for impingement heat transfer, Appl. Therm. Eng. 25 (2005) 31–44.
[27] C.W. Li, B. Zhu, A Sigma coordinate 3D k—ϵ model for turbulent free surface flow over a submerged structure, Appl. Math. Model. 26 (2002) 1139–1150.
[28] N.G. Wright, G.J. Easom, Non-linear k—ϵ turbulence model results for flow over a building at full-scale, Appl. Math. Model. 27 (2003) 1013–1033.
[29] Jamel Kechiche, Hatem Mhiri, Georges Le Palec, Philippe Bournot, Application of low Reynolds number k—ϵ turbulence models to the study of turbulent wall jets, Int. J. Therm. Sci. 43 (2004) 201–211.
[30] M.K. Patel, N.C. Markatos, An evaluation of eight discretization schemes for two-dimensional convection-diffusion equations, Int. J. Numer. Meth. Fluids 6 (1986) 129–153.
[31] S.K. Lele, Compact Finite Difference Schemes with Spectral-like Resolution, J. Comput. Phys. 103 (1992) 16–42.
[32] J.C. Kalita, Puneet Chhabra, An improved (9,5) higher order compact scheme for the transient two-dimensional convection diffusion equation, Int. J. Numer. Meth. Fluids 51 (2006) 703–717.
[33] T.K. Sengupta, S.K. Sirkar, A. Dipankar, High accuracy schemes for DNS and acoustics, J. Sci. Comput. 26 (2006) 151–193.
[34] K. Venkatasubbaiah, T.K. Sengupta, Mixed convection flow past a vertical plate: Stability analysis and its direct simulation, Int. J. Therm. Sci. 48 (2009) 461–474.
[35] Y.L. Chan, C.L. Tien, Numerical study of Two-Dimensional Laminar Natural convection in shallow open cavities, Int. J. Heat Mass Transfer 28 (1985) 612–630.
[36] H.N. Dixit, V. Babu, Simulation of high Rayleigh number natural convection in a square cavity using the lattice Boltzmann method, newblock Int, J. Heat Mass Transfer 49 (2006) 727–739.

[37] Y.S. Tian, T.G. Karayiannis, Low turbulence natural convection in an air filled square Cavity Part I: the thermal and fluid flow fields, Int. J. Heat Mass Transfer 43 (2000) 849–866.
[38] Koichi Ichimiya, Hideyuki Saiki, Behavior of thermal plumes from two-heat sources in an enclosure, Int. J. Heat Mass Transfer 48 (2005) 3461–3468.
[39] A. Mercer, H. Thompson, An experimental investigation of some further aspects of the Buoyancy-driven exchange flow between carbon dioxide and air following a depressurization accident in a magnox reactor, Part I: The exchange flow in inclined ducts, J. Br. Nucl. Energy Soc. 4 (1975) 327–334.